

Research Paper

Wavelet Analysis of Ultrasonic Lamb Wave Displacements in Three-Layer Adhesive Plates: Continuous Wavelet Transform (CWT) versus the Semi-Analytical Finite Element Method (SAFEM)

Abdelali YACOUBI¹*, Ayoub JABIRI¹, Mustapha AZKOUR²,
Rachid MANDRY¹, Mhammed EL ALLAMI^{1, 3}

¹) *Laboratory of Mechanics, IT, Electronics Telecommunications MIET
Department of Applied Physics, Faculty of Sciences and Techniques (FSTS)
Hassan I University*

Settat, Morocco; e-mail: a.yacoubi@uhp.ac.ma (A.Y.); a.jabiri@uhp.ac.ma (A.J.);
rachid.mandry@uhp.ac.ma

²) *Laboratory of Mechanics, Engineering and Innovation LM2I
National High School of Electricity and Mechanics (ENSEM)
Hassan II University*

Casablanca, Morocco; e-mail: mustapha.azkour.doc22@ensem.ac.ma

³) *Regional Center for Education and Training Professions (CRMEF)
Settat, Morocco; e-mail: MHAMMED.ELALLAMI@taalim.ma*

*Corresponding Author e-mail: a.yacoubi@uhp.ac.ma

In this paper, we aim to identify the most appropriate mother wavelet for analyzing the displacements of ultrasonic guided waves in tri-layered adhesive plates. We determine the group velocities of a given mode using various mother wavelets. The precision of each mother wavelet is evaluated by comparing the values of the group velocities with those found by the semi-analytical finite element method (SAFEM). The most appropriate mother wavelet function can then be used to study tri-layered adhesive plates with defects.

Keywords: Shannon wavelet; ultrasonic guided waves; bonded structures; signal processing; FEM.

1. INTRODUCTION

Non-destructive testing (NDT) is essential for maintaining safety and reliability across various industries, as it allows material integrity assessment without causing harm. This is especially crucial in the aviation sector, where safety is an

absolute necessity and regular maintenance of aircraft and their components is vital. Through the non-invasive detection of defects or anomalies, potential failures can be prevented, and maintenance practices can be optimized. Ultrasonic guided waves (UGWs) have been extensively used for thin structures due to their ability to travel long distances with low attenuation and sensitivity to the presence of small damages. For this purpose, dispersion curves are used to identify specific modes that can propagate at a given frequency [1]. The use of ultrasonic guided waves is critical for identifying defects and assessing the integrity of adhesive bonding to ensure optimal performance and structural robustness throughout the operational life [2]. To ensure this, it is necessary to post-process displacements obtained through experimentation or finite element (FE) software using effective methods, such as the continuous wavelet transform (CWT).

In the aerospace and automotive industries, tri-layered adhesive plates are widely used due to their lightweight nature and improved mechanical properties. The wavelet transform (WT) becomes a valuable mathematical tool for analyzing ultrasonic guided waves. It was DAUBECHIES [3] and NEWLAND [4] who first introduced wavelet analysis into the study of vibrational signals in the early 1990s. Initially, wavelet analysis was introduced to the time-frequency representation of transient waves propagating in a dispersive medium. HAYASHI *et al.* [5] estimated the thickness and elastic properties of metallic foils through wavelet analysis of laser-generated ultrasonic guided waves. JEONG and JANG [6] used the Gabor wavelet to draw an A0-mode dispersion curve in composite laminates. EL ALLAMI *et al.* [7, 8] investigated wavelet transform analysis for Lamb mode signals in plates to define the optimal mother wavelet. In the industrial sector, ultrasonic guided waves are frequently employed. Lamb waves can travel long distances without experiencing appreciable attenuation, which makes them ideal for large structures like plates, sheets, and other types of structures. In [7, 8], building on this foundation, a mother wavelet Shannon 1-1.5 was applied to a plate with internal defects to calculate energetic coefficients.

PAGET *et al.* [9] used a wavelet technique to detect damage in aerospace composites. The finite element method (FEM) is typically used for modeling the propagation of ultrasonic guided waves, resulting in displacement signals in the structure and their processing primarily created by the Fourier transform or, more recently, by the wavelet transform. When a structure is defective, the power coefficients of the reflected and transmitted ultrasonic guided modes by the defect can be calculated by post-processing the predicted displacement field using the CWT. The wavelet transform allows for the examination of signals in the time and frequency domains, enabling the detection and localization of defects in plates [10, 11]. Selecting an appropriate mother wavelet function is crucial for accurate and reliable results [12]. ZHAO *et al.* [13] conducted research on the detection of composite beam delamination using ultrasonic guided waves,

and the damage response signal was processed by the CWT. SHA *et al.* [14] studied delamination imaging in laminated composite plates using 2D wavelet analysis of guided wavefields. HAMEED *et al.* [15] used the CWT and, specifically, the Gabor wavelet to detect damage in a plate-like structure. FENG *et al.* [16] proposed a new method to detect delamination in composite structures using chirp-excited ultrasonic guided waves and wavelet transform. They used the Morlet mother wavelet and worked on carbon fiber reinforced plate (CFRP). LIU *et al.* [17] worked on the scale and translation parameters to optimize the Morlet wavelet and they applied their findings to a glass fiber epoxy composite plate.

The main objective of the present study is to assess the effectiveness of various mother wavelet functions in determining the group velocity of ultrasonic guided waves propagating in tri-layered adhesive plates. This will be accomplished by implementing a FE model using COMSOL Multiphysics software to compute the displacement field in tri-layered adhesive plates. Subsequently, by applying the wavelet transform process to the obtained displacements with a specially created MATLAB code, the group velocity will be obtained. Further, a comparative analysis will be performed to assess the accuracy of different wavelet functions and their outcomes versus the SAFE method. The findings of this study will provide valuable insights into the application of wavelet transforms and their utility in analyzing complex composite materials.

2. FORMULATION OF SAFE METHOD

By applying Hamilton's principle, the equation of motion is formulated using the SAFE method and solved numerically, considering an infinite elementary layer as shown in Fig. 1. This method combines the FEM with analytical expressions [18]. Specifically, the FEM is utilized to characterize the displacement field in the waveguide cross-section. For this particular case, the cross-section of the infinite elementary layer is sub-discretized using a 3-noded 1D element, and the wave is propagated in the longitudinal x -direction.

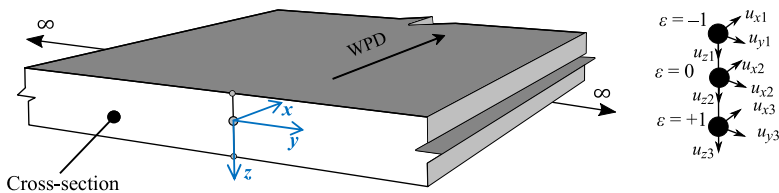


FIG. 1. Infinite elementary layer with three nodes (WPD – wave propagation direction).

The displacement field along the propagation direction is described analytically by a complex exponential function. Considering an infinitely wide structure

in the y -axis direction, its cross-section domain is subdivided into a system of multilayers modeled using 1D FEs with three nodes, as shown in Fig. 1. The displacement per element denoted by $u^{(e)}(x, z, t)$ is expressed in terms of shape functions matrix $\mathbf{N}(z)$, and the unknown nodal displacement for each element $q^{(e)}$ as follows:

$$(2.1) \quad u^{(e)}(x, z, t) = \mathbf{N}(z)q^{(e)}e^{i(kx-\omega t)},$$

where k is a complex wavenumber, $\omega = 2\pi f$ is the angular frequency, t is the time variable, and i is the imaginary unit. $\mathbf{N}(z)$ is defined as follows:

$$(2.2) \quad \mathbf{N}(z) = \begin{bmatrix} N_1(z) & 0 & N_2(z) & 0 & N_3(z) & 0 \\ 0 & N_1(z) & 0 & N_2(z) & 0 & N_3(z) \end{bmatrix},$$

with

$$(2.3) \quad N_1(z) = \frac{1}{2}z(z-1), \quad N_2(z) = 1-z^2, \quad N_3(z) = \frac{1}{2}z(z+1).$$

The strain ε can be represented as a function of the nodal displacements by using Eq. (2.1) as follows:

$$(2.4) \quad \varepsilon = \left[\mathbf{L}_x \frac{\partial}{\partial x} + \mathbf{L}_z \frac{\partial}{\partial z} \right] \mathbf{N}(z)q^{(e)}e^{i(kx-\omega t)} = (ikB_1 + B_2)q^{(e)}e^{i(kx-\omega t)},$$

where \mathbf{L}_x and \mathbf{L}_z express the strain parameters in matrix form and they are defined by:

$$(2.5) \quad \mathbf{L}_x = \begin{bmatrix} 0 & 0 \\ 0 & 1 \\ 1 & 0 \end{bmatrix}, \quad \mathbf{L}_z = \begin{bmatrix} 1 & 0 \\ 0 & 0 \\ 0 & 1 \end{bmatrix},$$

and

$$(2.6) \quad \mathbf{B}_1 = \mathbf{L}_x \frac{\partial \mathbf{N}}{\partial x}, \quad \mathbf{B}_2 = \mathbf{L}_z \mathbf{N}.$$

The stiffness and mass matrices for each element can be calculated in the elementary domain Ω_e as follows:

$$(2.7) \quad \begin{aligned} k_1^{(e)} &= \int_{\Omega_e} [\mathbf{B}_1^T \mathbf{C}_e \mathbf{B}_1] d\Omega_e, & k_2^{(e)} &= \int_{\Omega_e} [\mathbf{B}_1^T \mathbf{C}_e \mathbf{B}_2 - \mathbf{B}_2^T \mathbf{C}_e \mathbf{B}_1] d\Omega_e, \\ k_3^{(e)} &= \int_{\Omega_e} [\mathbf{B}_2^T \mathbf{C}_e \mathbf{B}_2] d\Omega_e, & m^{(e)} &= \int_{\Omega_e} [\mathbf{N}^T \boldsymbol{\rho}_e \mathbf{N}] d\Omega_e, \end{aligned}$$

where \mathbf{C}_e and ρ_e are the rigidity matrix and density of the elementary domain Ω_e , respectively, and \mathbf{T} is the transpose operator. These integrals are calculated numerically by using the Gaussian quadrature method between the limits of -1 and 1 on isoparametric elements, with full details available in the literature [19]. In order to accurately describe the dynamic behavior of the entire medium through its thickness, it is necessary to combine the mass and stiffness matrices of each element into four global matrices, which can be expressed as:

$$(2.8) \quad K_1 = \bigcup_{e=1}^{n_{el}} k_1^{(e)}, \quad K_2 = \bigcup_{e=1}^{n_{el}} k_2^{(e)}, \quad K_3 = \bigcup_{e=1}^{n_{el}} k_3^{(e)}, \quad M = \bigcup_{e=1}^{n_{el}} m^{(e)},$$

where n_{el} represents the total number of cross-sectional elements. These global matrices are then employed to reformulate the equation of motion within the cross-section as described below:

$$(2.9) \quad [K_1 + ikK_2 + k^2K_3 - \omega^2M] \mathbf{U} = 0,$$

where k is a complex wavenumber, $\omega = 2\pi f$ is the angular frequency, \mathbf{U} is the global vector of unknown nodal displacements, and i is the imaginary unit. K_1 , K_2 , K_3 , and M are defined in Eq. (2.8). A transformation is used by the SAFE method to simulate wave propagation in elastic waveguides and achieve a symmetric eigenvalue problem, as described by the following equation:

$$(2.10) \quad (\mathbf{A} - \omega^2\mathbf{M}) \mathbf{Q} = 0,$$

where

$$(2.11) \quad \mathbf{A} = \mathbf{K}_1 + k\widehat{\mathbf{K}}_2 + k^2\mathbf{K}_3, \quad \mathbf{Q} = \begin{bmatrix} \widehat{\mathbf{U}} \\ k\widehat{\mathbf{U}} \end{bmatrix},$$

noting that $\widehat{\mathbf{K}}_2$ is the \mathbf{K}_2 symmetric matrix and $\widehat{\mathbf{U}}$ is the new eigenvector. The group velocity can be directly calculated by using a well-known formula proposed by VIOLA *et al.* [18], which is

$$(2.12) \quad V_g = \frac{\phi_R^T K' \phi_R}{2\omega \phi_R^T M \phi_R}, \quad K' = \widehat{\mathbf{K}}_2 + 2kK_3,$$

noting that

$$(2.13) \quad \mathbf{T}^T \mathbf{K}_2 \mathbf{T} = -i\widehat{\mathbf{K}}_2,$$

where \mathbf{T} is the identity matrix, whose odd diagonal positions are replaced by the imaginary unit i , and ϕ_R denotes the right eigenvector of the system.

3. DISPERSION BEHAVIOR

The analysis of the dispersion behavior of tri-layered adhesive plates, as shown in Fig. 2, is conducted using SAFE method. Notably, the z -coordinate is parallel to the through-thickness direction of the structure, while the propagation direction is along the x -coordinate.

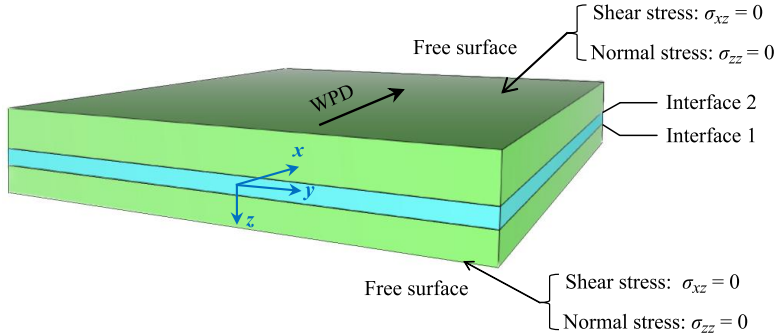


FIG. 2. Sample of the tri-layered adhesive plates (WPD – wave propagation direction).

To perform the numerical solution of the eigenvalue problem, a MATLAB code is established. The resulting dispersion curves are presented in terms of the wavenumber, group velocity, phase velocity and wavelength. Throughout the paper, the dispersion behavior of tri-layered adhesive plates is studied by considering the properties shown in Table 1.

Table 1. Mechanical and geometric properties of the tri-layered adhesive plates.

Layer	Material	Longitudinal velocity [m/s]	Transverse velocity [m/s]	Density [kg/m ³]	Thickness [mm]	Length [mm]
1	Aluminum	6150	3100	2700	3	750
2	Epoxy	771	370	1106	0.25	750
3	Aluminum	6150	3100	2700	3	750

Dispersion curves refer to the relationship between frequency and wave propagation characteristics, such as phase velocity or group velocity, in a given medium. The frequency has a significant impact on the dispersion curves, and even a minor change in frequency can change their behavior. This dispersive property is determined using the SAFE method. We use a mode separation approach based on the signs of displacement on the upper and bottom surfaces of the structure [20]. We decided to analyze multiple modes – there cannot be fewer than four – to conduct our investigation. To ensure an adequate examination,

we limited our study to 500 kHz. Within this frequency range, we identified two symmetrical modes, S0 and S1, and two antisymmetric modes, A0 and A1. It is important to keep in mind the shape of deformation and the thickness of the structure when the mode is excited to determine whether it is symmetric or antisymmetric. Furthermore, we can refer to the antisymmetric modes as bending modes and the symmetric modes as compression modes.

Figures 3 and 4 depict the profiles of wavenumber, group velocity, phase velocity and wavelength for a range of frequencies up to 500 kHz. It should be noted that when using the SAFEM, a minimum number of elements has to be used to generate all modes that must appear in a given frequency range [21], and the accuracy of solutions increases with the number of elements. For example, in the range of 3000 kHz, the minimum number of elements required is 18.

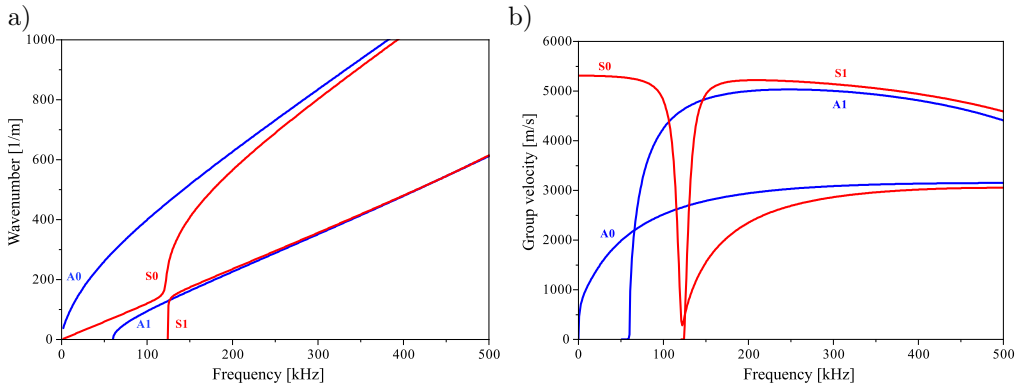


FIG. 3. Dispersion curves of tri-layered adhesive plates using the SAFE method: a) wavenumber, b) group velocity.

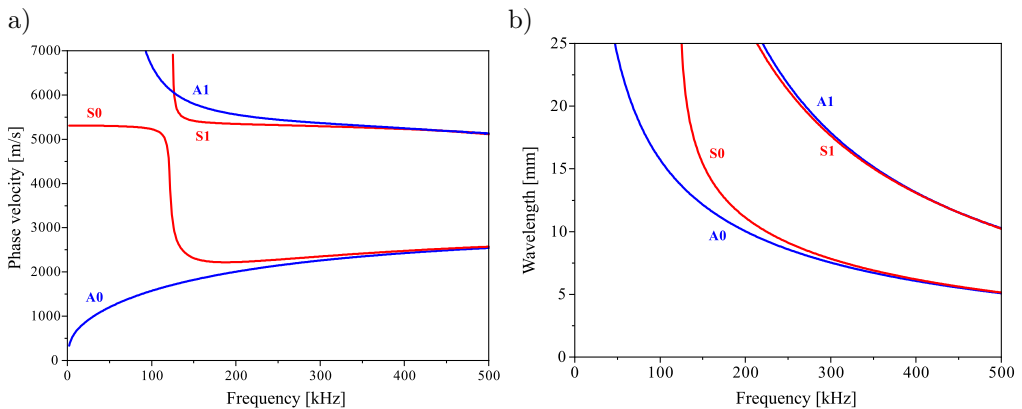


FIG. 4. Dispersion curves of tri-layered adhesive plates using the SAFE method: a) phase velocity, b) wavelength.

Three is the minimum number of elements for the maximum frequency range of 500 kHz. Each layer is regarded as a separate element. However, curves in Figs. 3 and 4 are calculated using six elements per layer. Yet, 120 elements are employed per layer when comparing the group velocities of the SAFE method with those determined by the CWT. This is used to approach analytical solutions with good accuracy, making the comparison more equitable.

4. POST-PROCESSING

4.1. Description of Lamb waves

Lamb waves propagate through solid plates [22]. They are elastic waves with particle motion occurring in the plane containing both the direction perpendicular to the plate and the direction of wave propagation. This type of ultrasonic wave was first described and analyzed by the English mathematician Horace Lamb in 1917. While there are only two wave modes that can travel in an infinite medium at the same velocity, plates can support two infinite sets of Lamb wave modes, the velocities of which are determined by the relationship between wavelength and plate thickness.

Since the 1990s, there has been a significant advancement in the understanding and application of Lamb waves due to the rapid increase in computing power availability. Significant practical use has been made of Lamb's theoretical formulations, particularly in the area of nondestructive testing.

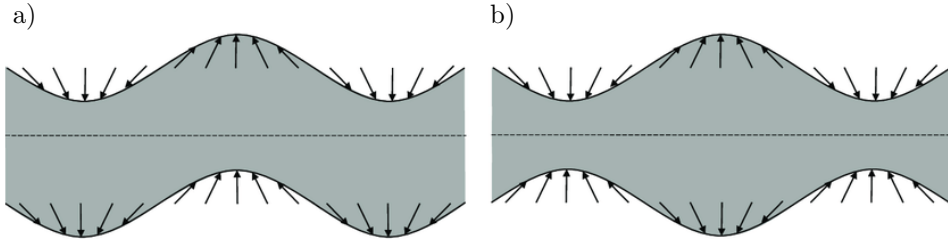


FIG. 5. Particle displacement of (a) antisymmetric (b) symmetric Lamb wave modes [23].

4.2. Wavelet analysis

Wavelet analysis is a powerful mathematical method for digital signal processing. It defines the signal process in the time-frequency domain using a set of basic functions. Linear combinations of modified and scaled functions can be represented by a wavelet family. The fundamental operations of a wavelet transform (WT) are waves produced by dilating and translating a mother wavelet. The wavelet transform is used to determine the arrival time of group velocity

by analyzing peak localization. So, the expression of the wavelet function [24] for the signal $u(t)$ is defined by:

$$(4.1) \quad Wf(a, b) = \frac{1}{\sqrt{a}} \int_{-\infty}^{+\infty} u(t) \Psi^* \left(\frac{t-b}{a} \right) dt,$$

where $\Psi(t)$ refers to the mother wavelet, $*$ denotes a complex conjugate, a is a dilation or scale parameter, and b is a translation parameter. In Eq. (4.1), a variety of wavelet functions can be applied.

4.3. Time of flight

The time of flight (TOF) represents the arrival time of the related wave packet to the receiver. Since the distance between transmitter and receiver is constant in all cases of the current research, it is possible to obtain the frequency-dependent group velocity $V_g(f)$ by using the following equation:

$$(4.2) \quad V_g(f) = \frac{d_2 - d_1}{t_2 - t_1}.$$

The WT, with the post-processing of displacement fields, identifies arrival times t_1 and t_2 for points Prob A and Prob B on the upper surface of the structure at propagation distances d_1 and d_2 , respectively (Fig. 5). This equation allows the calculation of the numerical group velocity at different frequencies. The time of flight can be extracted either experimentally or numerically, which is our target. A sensitivity analysis is then performed on the group velocity to validate its accuracy. The general test configuration of this study is shown in Fig. 6. The detection of data at working points Prob A and Prob B is also presented in Fig. 6. This particular set of data has been selected for specific frequency of 200 kHz as an example to illustrate several essential methodologies and results appearing from the time of flight extraction process.

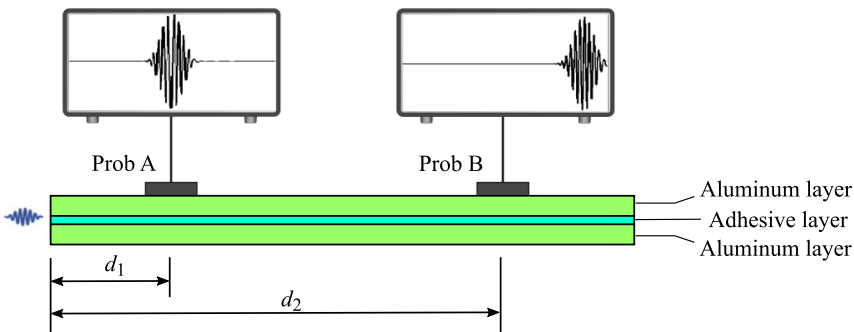


FIG. 6. Test configuration.

With the implementation of FE simulation, the displacements can be depicted as indicated in Fig. 6. The variances between the times of flight obtained from the wavelet transform approach and theoretical times are determined by using a set of mother wavelets.

5. NUMERICAL SIMULATION

5.1. Normalized displacement

The displacement field presents the variation of motion along the thickness of the structure. As we work in the sagittal plane (xoz) of the structure, which is parallel to the direction of wave propagation, we will have two displacements u_x and u_z . These displacements depend on the z variable and are expressed analytically by:

$$(5.1) \quad \begin{cases} u_x^{(j)} = [ik(A_j e^{iq_j z} + B_j e^{-iq_j z}) + is_j(C_j e^{is_j z} - D_j e^{-is_j z})] e^{i(kx - \omega t)}, \\ u_z^{(j)} = [iq_j(A_j e^{iq_j z} - B_j e^{-iq_j z}) - ik(C_j e^{is_j z} + D_j e^{-is_j z})] e^{i(kx - \omega t)}, \end{cases}$$

where A_j , B_j , C_j and D_j are constants of the layer j determined by applying the boundary conditions;

$$q_j = \sqrt{k_{L,j}^2 - k^2} \quad \text{and} \quad s_j = \sqrt{k_{T,j}^2 - k^2}$$

with

$$k_{L,j}^2 = \omega^2 / V_{L,j}^2 \quad \text{and} \quad k_{T,j}^2 = \omega^2 / V_{T,j}^2.$$

Here, ω is the angular frequency, $V_{L,j}$ and $V_{T,j}$ are the longitudinal and transverse velocities, respectively, for layer $j = 1, 2, 3$. By normalizing the displacement field with respect to the acoustic power, we can attain significant insights into the modes and their characteristics. The displacements are normalized by the acoustic power related to the quantity of energy delivered by ultrasonic guided waves. The displacement and stress profiles of the guided modes can be standardized by the acoustic power. Mathematical equations can be employed to obtain the expressions for the normalized displacements as follows:

$$(5.2) \quad u_{x,N} = \frac{u_x}{\sqrt{|P|}}, \quad u_{z,N} = \frac{u_z}{\sqrt{|P|}},$$

where P is the acoustic power utilized by a mode along the x -axis and perpendicular to the section defined in the ($yo z$) plane with a length of 1 meter along the y -axis and a total thickness of h along the z -axis, and it can be expressed as:

$$(5.3) \quad P = -\frac{1}{2} \text{Re} \left(\int_{-h/2}^{+h/2} (\mathbf{v}^* \cdot \boldsymbol{\sigma}) \mathbf{n} \, dz \right),$$

where \mathbf{n} is the normal to the elementary section $dydz$, $\boldsymbol{\sigma}$ is the stress tensor, v is the velocity vector and $*$ is the complex conjugate.

Figure 7 illustrates the normalized displacements at the frequency of 200 kHz for all existing modes. At this frequency, the dispersion curves illustrate four propagating modes: A0, S0, A1, and S1.

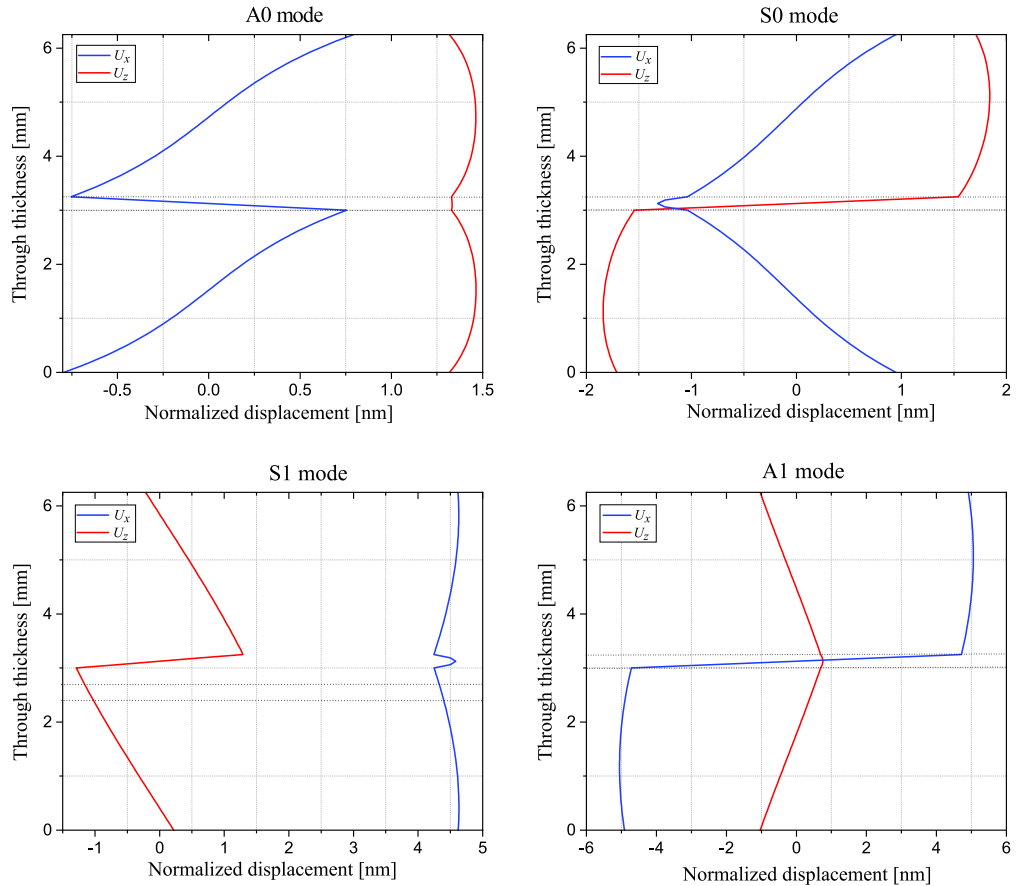


FIG. 7. Normalized displacement through the thickness of tri-layered adhesive plates.

5.2. Guided waves excitation

To acquire numerical displacements at the two probes A and B, the displacements are normalized and modulated by the Hann window to ensure the excitation at a set of selected frequencies ranging from 25 kHz to 262.5 kHz at the left edge of the tri-layered adhesive plates. An example of an excitation signal is presented in Fig. 8.

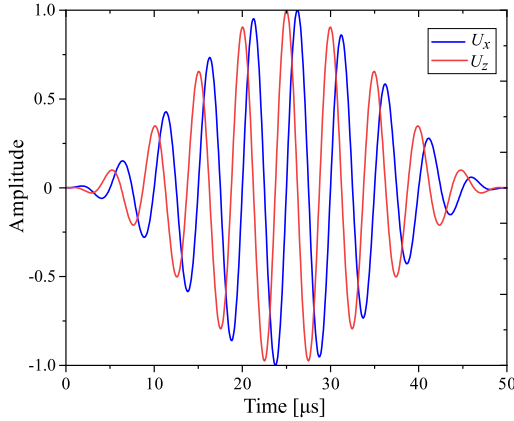


FIG. 8. A 10-cycle signal by a Hann window for A0 mode at 200 kHz.

5.3. Modeling guided waves propagation by FEM

The simulation employs a 2D FE model in COMSOL Multiphysics. The selection of parameters for the simulation's temporal and spatial steps requires specific proprieties to describe wave propagation accurately. The mesh assembly and temporal step conditions necessitate that the temporal step Δt must be sufficiently small to capture the dynamic behavior of the waves over time. It should be smaller than a critical value determined by the maximum wave velocity in the material and the spatial step size. By satisfying these spatial and temporal step conditions, the FE model in COMSOL can accurately capture the wave propagation characteristics and provide reliable results for the simulation of guided waves testing on tri-layered adhesive plates. The selection of mesh is an important factor in achieving accuracy in computational analysis. Precision is directly proportional to the number of sub-domains employed. Moreover, the number of nodes constituting each element is a key factor that significantly impacts the accuracy of calculations. An increase in the number of sub-domains of the mesh leads to an increase in the size of the system to be solved and, consequently, increases the overall computation time.

In order to mesh the structure under analysis, we choose to utilize an element size of 0.2 mm, which satisfies the following condition [25]:

$$(5.4) \quad \max(\Delta x, \Delta z) < \frac{\lambda_{\min}}{10}.$$

Here, we note that λ_{\min} represents the minimum wavelength. It is required that the size of the waveguide elements be less than one-tenth of the smallest wavelength of the modes that may propagate in the structure for computational

convergence to be achieved. For temporal discretization, the time step must satisfy the condition presented in [26]:

$$(5.5) \quad \Delta t < 0.7 \frac{\min(\Delta x, \Delta z)}{V_L}.$$

Satisfying the above condition, the time step is set to $\Delta t = 0.1 \mu\text{s}$, and the chosen frequency of 200 kHz is used to illustrate the temporal displacements in two probes for A0, S0, A1, and S1 modes. By focusing on this specific frequency, we can analyze and compare the displacement patterns over time for different modes. This allows us to gain insights into the propagation characteristics and mode-specific behavior of the waves at the selected frequency. The presented results provide an analysis of the temporal displacement, highlighting the variations in amplitude, phase, and shape in the two probes for each mode.

The profiles of displacements of all modes that can propagate at a frequency of 200 kHz in the tri-layered adhesive plates are shown in Fig. 9. The

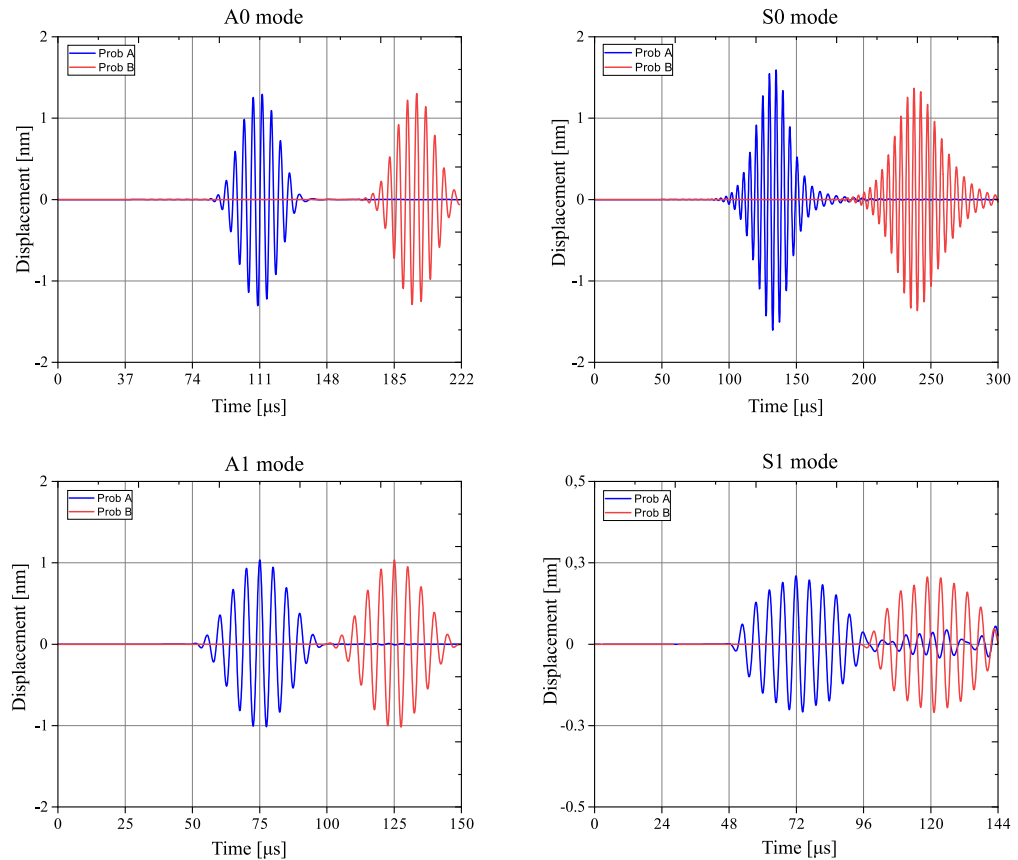


FIG. 9. Temporal displacements provided by simulations on tri-layered adhesive plates.

probes A and B depict normal displacements at the upper surface. It can be noted that these displacements are of the same order (nm) as those of the normalized displacements used for excitations. Knowledge of the amplitude of the displacement is essential since it determines the wave that will be more easily generated and/or detected during the inspection. The choice of the distance between the two probes is essential in this case to eliminate undesired reflection signals and guarantee reliable results. This distance was selected to give the wave packet enough room to travel before it encounters material constraints. We have represented the evolution of collected displacements as a function of time. The same procedure was executed for a range of frequencies between 25 kHz and 262.5 kHz. By applying the analysis to the entire frequency range of interest, we can observe and analyze the temporal displacements in the two probes for A0, S0, A1, and S1 modes. This provides insights into the displacement behavior, allowing us to identify variations in amplitude, phase, and shape for each mode.

5.4. Wavelet coefficient magnitude

The process for extracting group velocity information from the multimode guided wave signals must be applied after the displacement signals have been acquired. Figures 10 and 11 show the magnitude of the wavelet coefficients, using as examples, the mother wavelets “Shannon 1-1.5” and “Gaussian 1”, respectively, for the A0 mode at a frequency of 200 kHz. The amplitude of the coefficients acquired by wavelet analysis is denoted by the wavelet coefficient magnitude. It is possible to determine interesting changes in the modes at the chosen frequency by examining the wavelet coefficient magnitude. This strategy makes it easier to provide a quantitative measurement of the TOF of each peak.

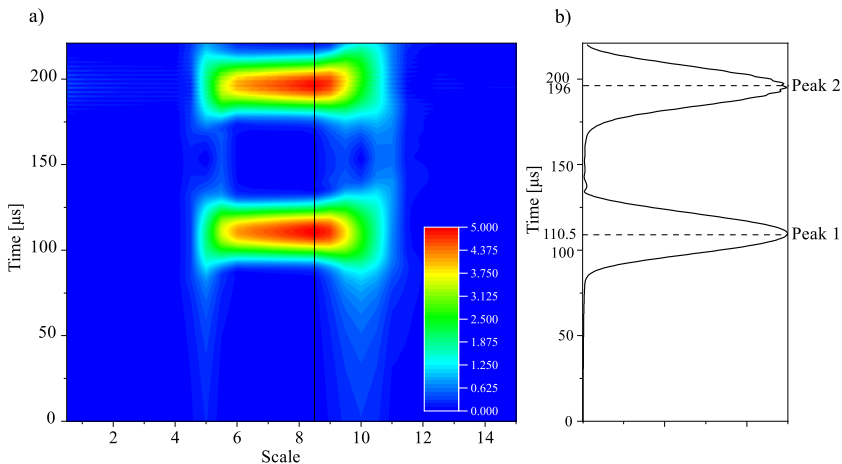


FIG. 10. a) “Shannon 1-1.5” wavelet coefficient of displacement, b) coefficient lines at probes A and B for the A0 mode at 200 kHz.

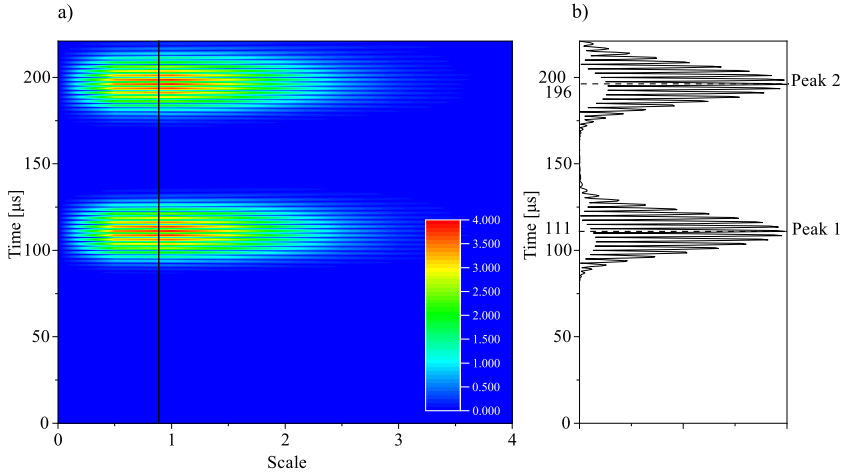


FIG. 11. a) “Gaussian 1” wavelet coefficient of displacement, b) coefficient lines at probes A and B for the A0 mode at 200 kHz.

In Fig. 10b, peak 1 and peak 2, correspond to the two arrival times of the incident A0 mode, t_1 and t_2 , respectively, with the first time being $t_1 = 110.5 \mu\text{s}$ and the second time is $t_2 = 196 \mu\text{s}$. Knowing that the distance between probe A and probe B is fixed at 250 mm and that the analytic group velocity of A0 mode is equal to 2927.249 m/s, it becomes possible to calculate the numerical group velocity by applying Eq. (4.2) and, subsequently, the relative error err . Then, by WT Shannon 1-1.5: $err = \mathbf{0.112\%}$. In Fig. 11b, the peak 1 corresponds to $t_1 = 111 \mu\text{s}$ and peak 2 corresponds to $t_2 = 196 \mu\text{s}$, which gives $err = \mathbf{0.476\%}$. It should be noted that when the analytical group velocity is very small and close to zero, calculating the relative error becomes challenging as it involves a ratio of two values that are both very small or very close to zero. It is probable that the relative error in this situation may not be representative. Additionally, launching numerical simulations can be difficult and time-consuming.

6. RESULTS AND DISCUSSION

A comparison between various mother wavelets regarding the relative error on the group velocity is conducted. The analysis covers all modes propagating in the frequency range from 25 kHz to 262.5 kHz. These simulations show the influence of the mother wavelet on the resulting error and reveal the effect of wavelet selection on the resulting group velocity values when coupling wavelet analysis results with those obtained from the SAFEM. The findings are important for guiding the precise selection of the suitable mother wavelet (see Figs. 12 and 13).

It should be noted that the average percentage error for any mother wavelet is calculated following these steps:

- 1) We first set the mode A0, A1, S0, or S1.
- 2) We calculate the absolute relative error (ARE) for each frequency in the range of 25–262.5 kHz. The following formula is used to calculate this:

$$(6.1) \quad \text{ARE} = \left| \frac{V_{g,\text{WT}} - V_{g,\text{SAFE}}}{V_{g,\text{SAFE}}} \right| \times 100,$$

where $V_{g,\text{WT}}$ is the group velocity calculated using WT and $V_{g,\text{SAFE}}$ is the group velocity calculated by SAFE method.

- 3) Finally, we compute the average of all the previously computed errors.

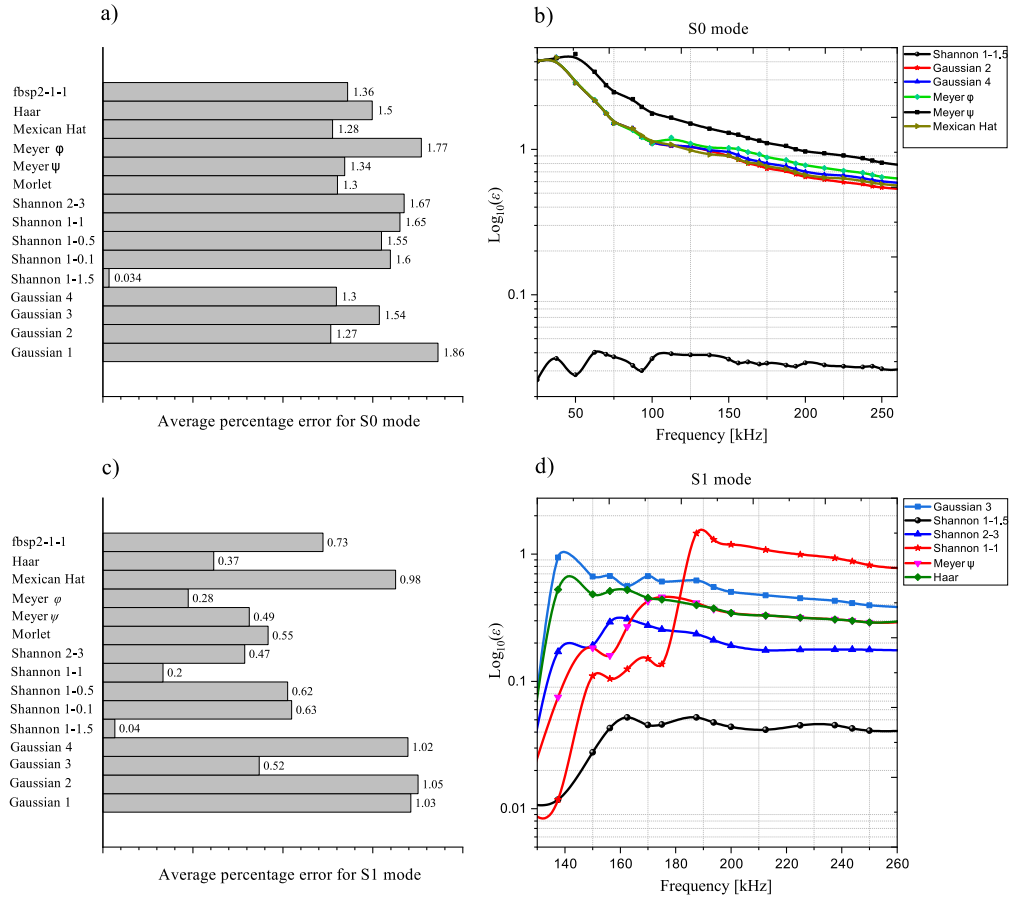


FIG. 12. Average percentage error for symmetric modes for different mother wavelets and relative error (err) evolution depending on frequency for the best mother wavelets.

The average error of all the wavelets for S0 and S1 modes is less than 2% over the entire considered frequency range (Figs. 12a and 12c). In particular, the Shannon wavelet 1-1.5 represents the minimum average error for both modes over the entire frequency range. Although the Shannon 1-1 wavelet represents a lower average error than Shannon 1-1.5 for the S1 mode over a small frequency range of 130–140 kHz (Fig. 12d), Shannon 1-1.5 remains five times more precise than Shannon 1-1 over the entire frequency range of 25–262.5 kHz.

For A0 and A1 modes, we note that the average error of all wavelets does not exceed 3% over the entire frequency range (Figs. 13a and c). However, Shannon 1-1.5 is the most suitable in terms of accuracy. The average error for A0 and A1 modes of all other wavelets tends to decrease as the frequency increases. On the other hand, the Shannon 1-1.5 error remains approximately constant (Figs. 13b and 13d). We see that fbsp2-1-1 comes in second position after Shannon 1-1.5 in terms of accuracy for A1 mode, but its average error is seventeen times higher

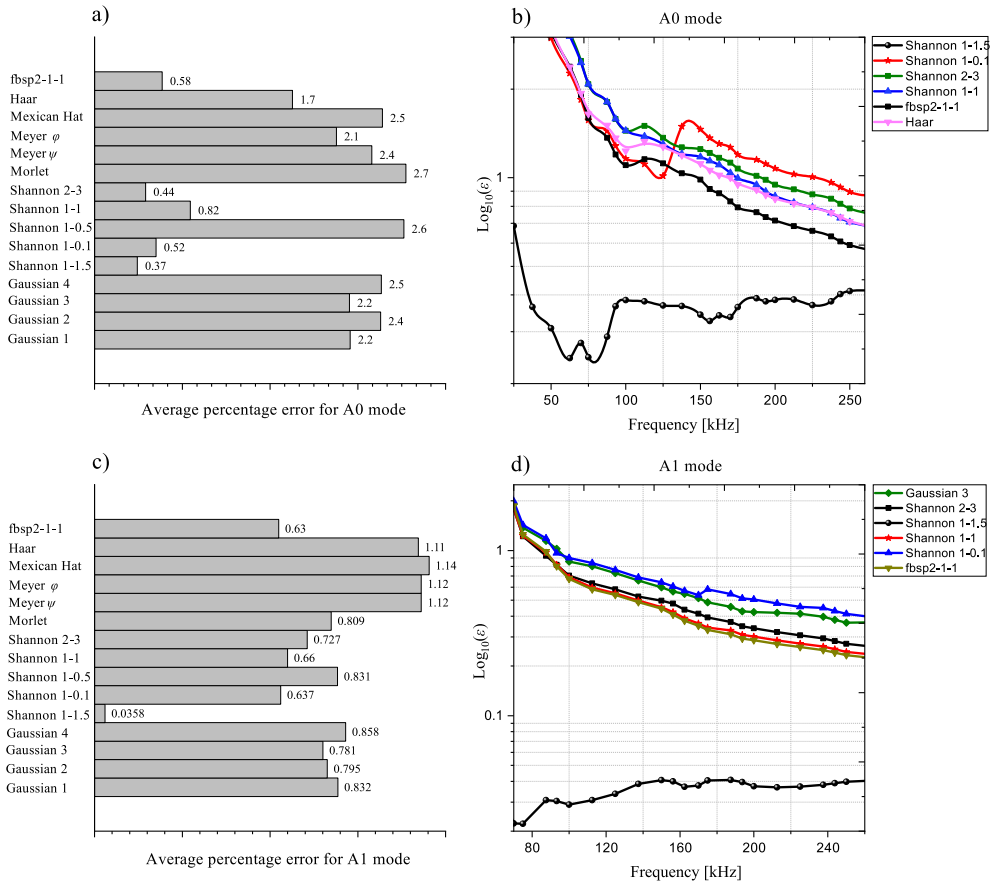


FIG. 13. Average percentage error for antisymmetric modes for different mother wavelets and relative error (err) evolution depending on frequency for the best mother wavelets.

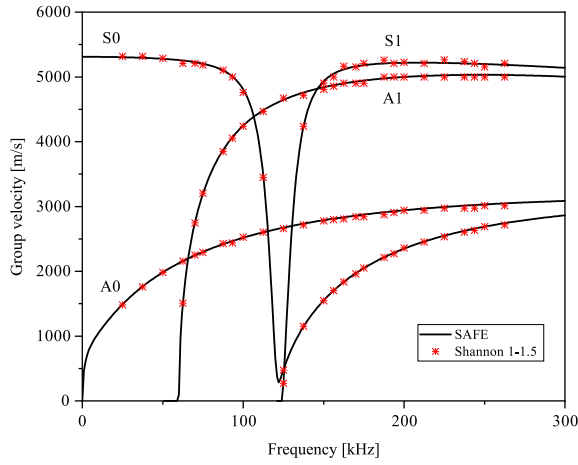


FIG. 14. Group velocity: WT Shannon 1-1.5 versus SAFE method.

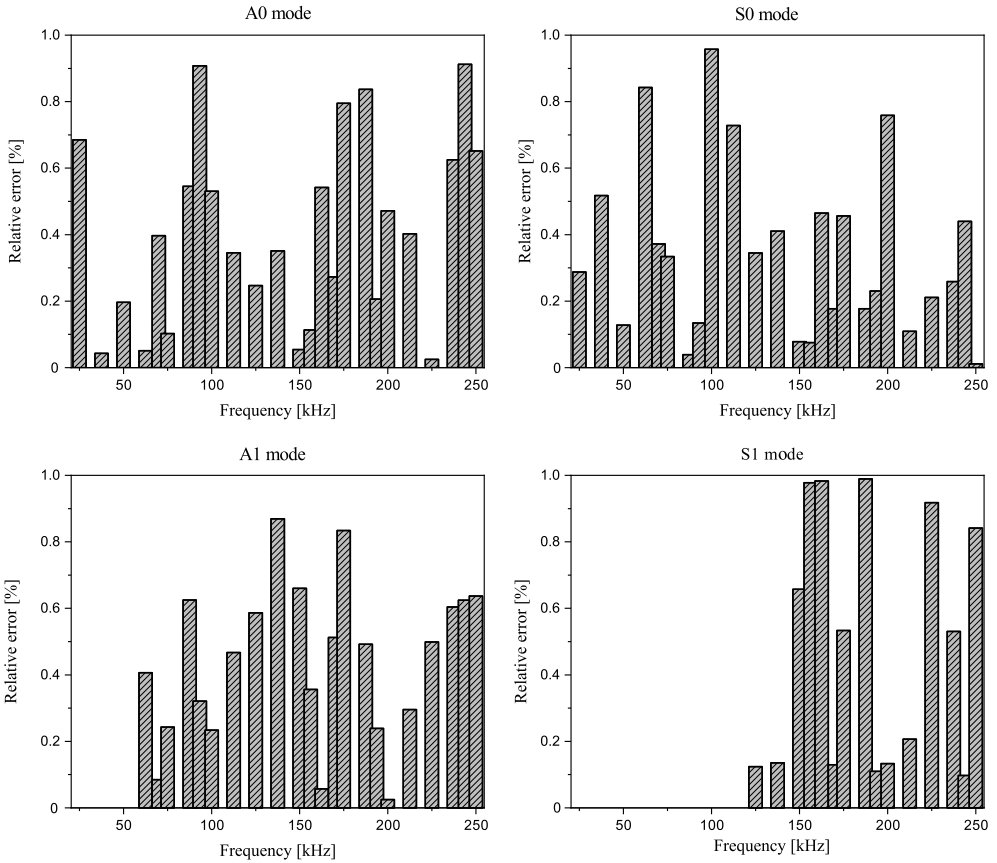


FIG. 15. Relative errors on the group velocity by WT Shannon 1-1.5.

than that of Shannon 1-1.5 over the entire frequency range. In general, we see that all the wavelets used in this study represent a fairly low error (<3%) for all modes and over the entire frequency range. But, if we demand precision, Shannon 1-1.5 appears the best choice. Since Shannon 1-1.5 is the most precise, we used it to draw the group velocity curves and superimpose them on those of SAFE method (Fig. 14).

The quantification of the relative error for each mode A0, A1, S0 and S1 on the considered frequency range using WT Shannon1-1.5 is presented in Fig. 15.

As a result, the relative error does not exceed 1% for all modes. However, it can be noted that the S0 mode presents the smallest average error as presented in Table 2.

Table 2. Average error per mode on the group velocity by WT Shannon 1-1.5.

Mode	A0	S0	A1	S1
Average error [%]	0.415	0.340	0.446	0.487

7. CONCLUSION

It should be noted that all mother wavelets studied, without exception, yield good results. However, we noticed that Shannon 1-1.5 presents a minimum error and is more precise than all the other wavelets. It should be mentioned that the main objective was no longer the calculation of dispersion curves but shifted to comparing the accuracy of different mother wavelet functions in determining the group velocity of ultrasonic guided waves propagating inside tri-layered adhesive plates. It can be also noted that, through this study, there is a very close link between the displacement of a point taken on the upper face of the structure and the dispersive behavior of the ultrasonic guided waves (UGWs). For simulations to be accurate and post-processing to yield acceptable results, execution times must be adhered to avoid unwanted reflection signals. For frequencies with group velocities that are too low or very close to zero, simulations become impossible given the runtimes, which become extremely long, and it should also be noted that if the meshing is done improperly, simulations can give erroneous or divergent results. The Shannon 1-1.5 wavelet can be used to calculate the energy coefficients of defective tri-layered adhesive plates, aiding in defect identification and mode sensitivity studies. Furthermore, it is possible to conduct a comparative study on theoretical, numerical, and experimental results.

AUTHOR CONTRIBUTIONS

Author 1 planned the scheme and initiated the project; Author 2 analyzed the numerical results; Author 3 developed the mathematical modeling and ex-

amined the theory validation; Author 4 and Author 5 directed and supervised the project. The manuscript was written with the contributions of all authors. All authors discussed the results, reviewed, and approved the final version of the manuscript.

ACKNOWLEDGMENTS

Not applicable.

CONFLICT OF INTEREST

The authors declare no potential conflicts of interest concerning the research, authorship, and publication of this article.

FUNDING

The authors received no financial support for the research, authorship, and publication of this article.

DATA AVAILABILITY STATEMENTS

The datasets generated and/or analyzed during the current study are available from the corresponding author on reasonable request.

REFERENCES

1. ZHANG X., YUAN S., HAO T., Lamb wave propagation modeling for structure health monitoring, *Frontiers of Mechanical Engineering in China*, **4**(3): 326–331, 2009, doi: 10.1007/s11465-009-0045-6.
2. MALINOWSKI P.H., ECAULT R., WANDOWSKI T., OSTACHOWICZ W.M., Evaluation of adhesively bonded composites by nondestructive techniques, [in:] *Proceedings Volume 10170, Health Monitoring of Structural and Biological Systems 2017; SPIE Smart Structures and Materials + Nondestructive Evaluation and Health Monitoring*, 2017, doi: 10.1117/12.2259852.
3. DAUBECHIES I., The wavelet transform, time-frequency localization and signal analysis, *IEEE Transactions on Information Theory*, **36**(5): 961–1005, 1990, doi: 10.1109/18.57199.
4. NEWLAND D.E., Wavelet analysis of vibration: Part 1 – Theory, *Journal of Vibration and Acoustics*, **116**(4): 409–416, 1994, doi: 10.1115/1.2930443.
5. HAYASHI Y., OGAWA S., CHO H., TAKEMOTO M., Non-contact estimation of thickness and elastic properties of metallic foils by laser-generated Lamb waves, *NDT & E International*, **32**(1): 21–27, 1999, doi: 10.1016/S0963-8695(98)00029-2.

6. JEONG H., JANG Y.-S., Wavelet analysis of plate wave propagation in composite laminates, *Composite Structures*, **49**(4): 443–450, 2000, doi: 10.1016/S0263-8223(00)00079-9.
7. EL ALLAMI M., RHIMINI H., NASSIM A., SIDKI M., Application of the wavelet transform analysis to Lamb modes signals in plates, *Electronic Journal «Technical Acoustics»*, **8**: 1–10, 2010.
8. EL ALLAMI M., RHIMINI H., SIDKI M., Application of the complex mother wavelet Shan 1-1.5 processing to Lamb modes signals in plates, *International Journal of Science and Research (IJSR)*, **4**(1): 1849–1854, 2015.
9. PAGET C.A., GRONDEL S., LEVIN K., DELEBARRE C., Damage assessment in composites by Lamb waves and wavelet coefficients, *Smart Materials and Structures*, **12**(3): 393, 2003, doi: 10.1088/0964-1726/12/3/310.
10. ZIMA B., RUCKA M., Application of wavelet transform in analysis of guided wave propagation signals for damage detection in a steel plate, *Diagnostyka*, **16**(2): 43–48, 2015.
11. DOUKA E., LOUTRIDIS S., TROCHIDIS A., Crack identification in plates using wavelet analysis, *Journal of Sound and Vibration*, **270**(1-2): 279–295, 2004, doi: 10.1016/S0022-460X(03)00536-4.
12. LI F., MENG G., KAGEYAMA K., SU Z., YE L., Optimal mother wavelet selection for Lamb wave analyses, *Journal of Intelligent Material Systems and Structures*, **20**(10): 1147–1161, 2009, doi: 10.1177/1045389X09102562.
13. ZHAO G., WANG B., WANG T., HAO W., LUO Y., Detection and monitoring of delamination in composite laminates using ultrasonic guided wave, *Composite Structures*, **225**: 11161, 2019, doi: 10.1016/j.compstruct.2019.111161.
14. SHA G., RADZIENSKI M., SOMAN R., WANDOWSKI T., CAO M., OSTACHOWICZ W., Delamination imaging in laminated composite plates using 2D wavelet analysis of guided wavefields, *Smart Materials and Structures*, **30**(1): 015001, 2021, doi: 10.1088/1361-665X/abc66b.
15. HAMEED M.S., LI Z., ZHENG K., Damage detection method based on continuous wavelet transformation of Lamb wave signals, *Applied Sciences*, **10**(23): 8610, 2020; doi: 10.3390/app10238610.
16. FENG B., RIBEIRO A.L., RAMOS H.G., A new method to detect delamination in composites using chirp-excited Lamb wave and wavelet analysis, *NDT & E International*, **100**: 64–73, 2018, doi: 10.1016/j.ndteint.2018.08.004.
17. LIU B., LIU T., MENG F., Research on Morlet wavelet based Lamb wave spatial sampling signal optimization method, *Journal of Shanghai Jiaotong University*, **23**(Suppl 1): 61–69, 2018, doi: 10.1007/s12204-018-2024-8.
18. VIOLA E., MARZANI A., BARTOLI I., Semi-analytical formulation for guided wave propagation, [in] Elishakoff I. [Ed.], *Mechanical Vibration: Where do we Stand?*, International Centre for Mechanical Sciences, Vol. 488, pp. 105–121, Springer, Vienna, 2007, doi: 10.1007/978-3-211-70963-4.6.
19. ROSE J.L., *Ultrasonic Guided Waves in Solid Media*, Cambridge University Press, New York, 2014.
20. ZITOUNI I., RHIMINI H., CHOUAF A., Comparative study of the spectral method, DISPERSÉ and other classical methods for plotting the dispersion curves in anisotropic

- plates, *Journal of Applied and Computational Mechanics*, **9**(4): 955–973, 2023, doi: 10.22055/jacm.2023.42530.3941.
21. GALÁN J.M., ABASCAL R., Numerical simulation of Lamb wave scattering in semi-finite plates, *International Journal for Numerical Methods in Engineering*, **53**(5): 1145–1173, 2001, doi: 10.1002/nme.331.
 22. LAMB H., On the vibrations of an elastic sphere, *Proceedings of the London Mathematical Society*, **s1-13**(1): 189–212, 1881, doi: 10.1112/plms/s1-13.1.189.
 23. VÁZQUEZ S., GOSÁLBEZ J., BOSCH I., CARRIÓN A., GALLARDO, C., PAYÁ J., Comparative study of coupling techniques in Lamb wave testing of metallic and cementitious plates, *Sensors*, **19**(19): 4068, 2019, doi: 10.3390/s19194068.
 24. GRAPS A., An introduction to wavelets, *IEEE Computational Science & Engineering*, **2**(2): 50–61, 1995, doi: 10.1109/99.388960.
 25. NG C.T., VEIDT M., ROSE L.R.F., WANG C.H., Analytical and finite element prediction of Lamb wave scattering at delaminations in quasi-isotropic composite laminates, *Journal of Sound and Vibration*, **331**(22): 4870–4883, 2012, doi: 10.1016/j.jsv.2012.06.002.
 26. VEIDT M., NG C.T., Influence of stacking sequence on scattering characteristics of the fundamental anti-symmetric Lamb wave at through holes in composite laminates, *The Journal of the Acoustical Society of America*, **129**(3): 1280–1287, 2011, doi: 10.1121/1.3533742.

Received November 11, 2023; accepted version April 17, 2024.

Online first May 21, 2024.



Copyright © 2024 The Author(s).
Published by IPPT PAN. This work is licensed under the Creative Commons Attribution License
CC BY 4.0 (<https://creativecommons.org/licenses/by/4.0/>).